

CONTROL OF A SWEEP WING TAILLESS AIRCRAFT THROUGH WING MORPHING

R. W. Guiler* and W.W. Huebsch**

***Aurora Flight Sciences, Bridgeport, WV**

****West Virginia University, Morgantown, WV**

Keywords: *wing morphing, tailless swept wing, UAV*

Abstract

Inspired by flight in nature, the work done by Lippisch, the Hortens, and Northrop offered insight to achieving the efficiency of bird flight with swept-wing tailless aircraft. Tailless designs must incorporate aerodynamic compromises for control, which have inhibited potential advantages. A morphing mechanism, capable of adaptively changing the twist of the wing and that can also provide pitch, roll and yaw control for a tailless swept wing aircraft is the first step in a series of morphing techniques, which will lead to more fluid, bird-like flight. This research focuses on investigating the design of a morphing wing to improve the flight characteristics of swept wing Horten-type tailless aircraft. Flight demonstrators, wind tunnel flow visualization, wind-tunnel force and moment data along with CFD studies have been used to evaluate the stability, control and efficiency of a morphing swept wing tailless aircraft. This new control technique was experimentally and numerically compared to an existing elevon equipped tailless aircraft and has shown the potential for significant improvement in efficiency. The feasibility of this mechanism was also validated through flight testing of a flight demonstrator. In the process of comparing the elevon equipped aircraft and the morphing model, formal wind tunnel verification of wingtip induced thrust, found in Horten (Bell Shaped Lift distribution) type swept wing tailless aircraft was documented. A more complete physical understanding of the highly complex flow generated in the control region of the morphing tailless aircraft has been developed.

1 Introduction

When looking at the efficiency and elegance of bird flight in nature our aviation achievements seem to pale in comparison. Inspired by a gliding tree seed called *Zanonia* (*Macrocarpa*) and the flight of seagulls, work done by Alexander Lippisch, Reimar and Walter Horten, and John Northrop offered a chance at achieving some of the efficiency of bird flight with swept wing tailless aircraft.

Swept wing tailless aircraft exhibit a highly efficient configuration with low parasitic drag, and up to 30% less total drag. A minimum of two control surfaces are needed for pitch, roll and yaw. Propulsion, fuel and payload are all built into the wing structure, which allows the design of a very lightweight rigid structure [1]. Finally the smooth lines with very few protrusions allow the design of an aircraft with a minimum electromagnetic signature, which has become very important to today's military operations. When considering unmanned aerial vehicles (UAVs) a tailless aircraft not only has the above mentioned advantages but due to their geometry they can be easily folded into small containers for military or planetary exploration type missions.

Unfortunately, there are a number of design compromises necessary for tailless aircraft, which currently do not allow them to exploit many of their potential advantages.

A major aerodynamic/control problem with swept wing tailless aircraft is adverse yaw. Adverse yaw can be explained as a result of induced drag. When initiating a turn the elevon movement on the outboard wing increases lift and induced drag on that wing. This increases

the adverse yaw, which drags the up-moving wing aft, opposite to the desired yaw direction [2]. Alexander Lippisch recognized in the 1930's the effects washout (wing twist with the leading edge of the wing tip having a negative angle when compared to the root airfoil) had on adverse yaw. Lippisch originally used washout toward the wing-tips to reduce the risk of tip stalls, when he also observed a reduction in the effects of adverse yaw when maneuvering. Through the study of hundreds of model gliders and a large variety of tailless manned gliders and motor gliders, Reimar Horten developed the use of a bell shaped lift distribution for swept wing tailless aircraft as a cure for adverse yaw in the 1930's. Horten theorized that if you use a bell shaped lift distribution, instead of an elliptical lift distribution, adverse yaw would be minimized. This bell-shaped lift distribution is developed using wash-out of the wing. In a coordinated turn a down elevon position close to the wing tip increases the lift vector of the washed-out section of wing which effectively produces a small amount of induced thrust at the wing tip negating the increased induced drag that causes adverse yaw. In theory this works, but there have been no formal studies which have confirmed this and Hortens own test pilots including Dr. Karl Nickel and Heinz Scheidhauer indicate that most of the Horten designs suffered from adverse yaw problems.

The flow physics in the tip region of a swept wing tailless aircraft are very complex and poorly understood with crossflow and a large upwash from relatively large root section of the wing. Other tailless aircraft designers have chosen to use winglets or up elevon on one side plus dihedral effect on the opposite to induce rolling and drag rudders for yaw as a solution, but many of these solutions produce additional drag.

Tailless aircraft have a narrow center of gravity (cg) range. Any variations from design cg must be trimmed using control surfaces. Tailless aircraft that only use elevons for trim are susceptible to dangerous tip stalls (risk minimized using built in wash out). Extreme elevon throws can initiate separated flow at the wing tips and cause a tip stall. This is also

aggravated when elevons are used for trim for cg compensation.

In the late 1950's the Astrophysics Department of Mississippi State University and Dezo George Falvy conducted a thorough aerodynamic study of the Horten IV tailless sailplane. This study concluded that the aircraft could be redesigned to achieve a theoretical glide ratio of close to 50:1. Then many of the poor handling characteristics could be remedied if there was a way to adjust the washout in flight [3]. Dr. Reimar Horten and Dr. Karl Nickel also came to a similar conclusion [4]. The Hortens and Nickel also mathematically modeled elevon control inputs as effective washout [5].

Wing morphing technology offers us the opportunity to do away with many of the design compromises inherent for the control of swept wing tailless aircraft. Tailless aircraft will finally be able to approach the aerodynamic efficiencies envisioned by the pioneers in tailless aircraft. Enhanced control and maneuverability are also possible benefits of wing morphing.

Wing morphing can immediately address the design compromise of using fixed washout or large winglets in swept wing tailless aircraft. Active morphing of the wing as adaptive washout allows washout to be used only when maneuvering. This eliminates the corresponding increased drag for all non-maneuvering flight regimes.

2 Details of Research

This research has focused on improving the handling characteristics, expanding the flight envelope and increasing the efficiency of swept wing tailless aircraft using wing-morphing technology. This research has also allowed some insight into the flow physics which are generated around an adaptive washout morphing wing.

Phase 1 research allowed the experimental comparison of an existing state of the art tailless wing design with a design using wing morphing (adaptive washout). This phase also explored operational characteristics, handling, stall performance, and efficiency of a swept wing tailless aircraft utilizing wing morphing

technology through the use of wind tunnel testing and UAV flight demonstrators.

Phase 2 of this research developed multiple CFD models that recreate the experimental aerodynamic data on the morphing design to better understand the flow physics. These CFD models have been used to explore the pressure and flow fields surrounding various morphed wing configurations.

2.1 Geometry/Aerodynamics

The WVU project began with the assumption that the Horten-Panek PUL 10 is a state-of-the-art Horten-type swept wing tailless aircraft. The PUL-10 is a very efficient well handling two place tailless general aviation aircraft. This design was used as a basis for the aircraft aerodynamics in this project. The basic planform, controls and washout were a starting point and then adapted based on scale considerations, remote control aircraft conventions and fabrication-based constraints. Through the process of developing a wing morphing mechanism for control, comparisons in performance were made back to the PUL-10 type wind-tunnel model. The PUL-10 was designed with a sweep of 35 degrees and washout combination to develop a bell shaped (lift distribution proportional to $(\sin^3 x)$) lift distribution to counteract adverse yaw during maneuvering.

The airfoil combination of the PUL-10 has been modified from the original to a modified Horten II airfoil called the MH-78 at the root and the NACA 0010 at the tip. The MH-78, designed by Martin Hepperle, has better performance than the original Horten airfoil at the low Reynolds numbers associated with the wind tunnel models and the flight demonstrators [6]. The tip airfoil was changed from the Horten Symmetric 10%, to the NACA 0010. The shape and performance of these airfoils are almost identical. The NACA 0010 was chosen because it is widely used and there is a wealth of literature written about its performance.

Two swept wing models were developed for wind tunnel testing – one with a standard elevon and one with the morphing adaptive washout. The non-morphing model used for

comparison was simplified to allow available construction techniques to be used in the construction of the models. Four degrees of dihedral was built into the models for stability.

Glider and RC model testing with the aerodynamic configuration shown in Fig. 1 were used to collect performance data to compare to the morphing models.

2.2 Morphing Mechanism

Study of early tailless designs and approximation techniques led to the conclusion that varying the twist in the outboard sections of a wing can develop the desired control forces needed for maneuvering flight. The Wright brothers demonstrated this with their wing warping controls; this also has been proven by mathematical models used by the Horten's and Karl Nickel that modeled control force changes as changes in twist. Most of the twist and control surfaces in Horten aircraft are located in the outer 1/3 of the wing, so it was decided in the current work to allow the entire outer 1/3 of the wing to change twist in the initial morphing models.

There are two requirements of a morphing wing structure, which are opposed to each other. The first is that the structure needs to be flexible enough to allow significant shape change with minimal actuation forces. The second requirement is that the wing structure needs to be rigid enough to maintain a predictable aerodynamic shape in the presence of aerodynamic loads.

A common problem with aircraft wing structures is flutter, which is an oscillation caused by aerodynamic forces. This is a much more serious problem with aircraft that have very light-weight structures or high aspect ratio wings. The design of a morphing structure which must be rigid at all times yet is free to assume a new shape with a reasonably sized actuation force is a major problem. There are a number of new actuator technologies, which offer some help in this matter, piezo-electric membranes or shape memory alloy actuators. When these actuator technologies are embedded in a composite structure they may solve the structural problems of morphing aircraft, but

both technologies are very immature, lack the range of motion needed for the power available, time scales may be too large, and are currently cost prohibitive.

The WVU first generation morphing design depended on a composite skin and a carbon actuator rod to provide the resistance to aerodynamic forces. It should be noted that for brevity, many of the lessons learned and solutions found for the morphing mechanism are not included in this paper, but can be found in great detail from Guiler [7].

Initial wind tunnel testing indicated that a number of improvements needed to be made to the morphing wing mechanism. In an attempt to reduce flutter and improve the operation of the adaptive washout morphing mechanism each of the free floating wing sections had a 20% increase in the bearing area between them and the other wing sections. To improve both durability and ability to resist ballooning at low pressures found on the upper wing surface the Latex skin was replaced by a slightly thicker Neoprene skin.

Improving the actual shape of the morphing portion of the wing during control changes was a goal when it was decided to replace the Teflon™ coated steel restraining cable in the wing trailing edge with a Nylon monofilament [7]. The Nylon monofilament has better elastic and friction properties than the steel cable. This replacement smoothed out the curvature of the trailing edge during morphing and was responsible for a 12% drop in needed actuation torque. The improved adaptive washout morphing mechanism can be seen in Fig. 2. The new trailing edge shapes can be seen in Fig. 3 with control positions and deflections given in Table 1.

The elevon equipped PUL-10 type wing remained unchanged. The five control positions on both models were adjusted so that either the elevon or the tip of the morphing wing were at 0, -3.5, -7, 3.5 and 7 degree angle of attack (AOA) from their neutral position. Elevon AOA was measured from the hinge line aft and on the morphing model tip deflection was measured from the leading edge aft (see Table 1). Angle of attack for both of the wind tunnel models was changed by rotating the models around the force

balance and reattaching the models at the desired angle of attack.

Table 1. Control positions and deflections for both wings

| Control Position | Elevon Deflection Degrees | Morphing deflection degrees |
|------------------|---------------------------|-----------------------------|
| 1 | 0 | 0 |
| 2 | 3.5 | -3.5 |
| 3 | 7 | -7 |
| 4 | -3.5 | 3.5 |
| 5 | -7 | 7 |

2.3 Wind Tunnel Testing

Wind tunnel experiments were conducted on both the elevon and morphing wing models. The primary quantitative data was obtained from a 6-component balance, but flow visualization was also performed. The 6-component balance has been used to acquire lift, drag, pitch, yaw and roll data (see [7] for full details).

In order to validate the procedures and experimental setup of the WVU wind tunnel it was desirable to conduct a validation study where a good quality published data set was matched in the WVU tunnel. The WVU wind tunnel has a current velocity limitation of approximately 50 m/s. The study which was chosen for a test case is a study conducted by Gerontakos and Lee [8]. Their study provided tip and wake vorticity data as well as coefficient of lift and drag data for a swept NACA 0015 wing and a NACA 0015 wing with square tips and an aspect ratio of 2.5.

The WVU NACA 0015 model has a square tip geometry and was studied at various AOAs at a Reynolds number of 1.83×10^5 . Force and moment data was collected using the six component balance. Data collected for the WVU tunnel is compared to [8] (e.g. Fig. 4). There was good agreement between coefficient of lift data and reasonable agreement for the drag data. There was a small Reynolds number difference between the two data sets. The WVU data set was collected at 183,000 and [8] was collected at 181,000. This normally would be insignificant, but from previous tests at WVU this Reynolds number range has shown there to

be large variations in lift and drag values with small variations of Re.

Wind tunnel testing collected basic forces and moments for both the elevon equipped model and the morphing model. Both were tested at 32 ft/sec (10 m/s), 49 ft/sec (15 m/s) and 68 ft/sec (21 m/s) and 0, 3.5 and 7 degree angle of attack (AOA) in the 32 x 45 inch test section in the WVU wind tunnel. The Reynolds numbers ranged between 186,000 and 375,000.

The average of three sets of six raw load and moment data points were collected from the force balance for each test. These numbers which correspond to lift, drag, pitch, roll and yaw were adjusted for any balance related interactions. The forces and moments were then converted to nondimensional coefficients for comparison. Lift (C_L) and Drag (C_D) coefficients were nondimensionalized using the wing area of 1.317 sq. feet. Pitching moment (C_{mP}) was nondimensionalized using the wing area times the mean aerodynamic cord (MAC) of 0.731 ft., Roll (C_{mR}) and yaw (C_{mY}) were nondimensionalized using the wing area times the model span of 2.0 ft. The force and moment behavior between the elevon and morphing wings were similar. The morphing wing displays slightly higher C_L and lower C_D values.

Fig. 5 compares C_L and C_D values of both wings at 0 degrees angle of attack and 21 m/s and Fig. 6 these values at 7 degrees angle of attack and 21 m/s. The behavior of these curves changes dramatically as lift increases, either with increased angle of attack or increased tunnel velocity. Data was acquired at 10, 15 and 21 m/s, but the basic control behavior of these wings appears to change between 15 and 21 m/s or between Reynolds numbers of 280,000 and 370,000. The actual performance of these wings can be seen more clearly by comparing the lift over drag (L/D) ratios at the various control positions as seen in Fig. 7. Even though the wings were mounted parallel to the centerline of the test section, the negative C_L at 0 degree AOA for the morphing wing may indicate that the actual orientation of the wings to the flow give a slight negative AOA.

The behavior of yaw moments is very important to the control of any aircraft and is of particular interest when dealing with a tailless

aircraft. At zero AOA the yaw behavior of both wings appeared to be opposite with much larger yaw changes and a reversal of yaw moment in the morphing wing. The yaw behavior of both wings became much more similar at 3.5 and 7 degrees AOA with the interesting point that at control positions 4 and 5 the yaw moment was strongly negative. Control positions 4 and 5 were the positions with the highest lift. This same unusual behavior was seen in the C_D of both wings as lift increased. This behavior was not seen at 10 and 15 m/s. This may indicate a Reynolds (Re) number dependence. A full set of data for the elevon wing was collected at 26 m/s and $Re = 493497$ to show that the trends seen at 21 m/s remain at 26 m/s.

Various flow visualization techniques were experimented with in order to better understand the flow on the outer third of both wing models. Smoke flow visualization has the potential of significantly aiding the understanding of the flow in these tailless models. While many new techniques were developed very little was learned about the flow structure. The models were also tufted using polyester tufts on a 1.5 inch grid. Both the elevon and morphing models were filmed at 68 ft/sec (21 m/s) through all five control positions and with the wing at 7 degrees angle of attack.

Observations under these conditions showed that the majority of the flow was laminar. The onset of separated flow started to become visible at the root of the elevon wing at control position 5. The tip vortices were clearly seen with tufts. The tip vortex on the elevon wing disappeared between control position 1 and 2. When facing the leading edge left wing wind tunnel model the vortices were counter clockwise at control position 3 and clockwise at control positions 3, 4 and 5. The tip vortex on the morphing wing disappeared at control position 2. When facing the leading edge left wing wind tunnel model the vortices were counter clockwise at control position 3 and clockwise at control positions 1, 4 and 5. Although it was difficult to quantify, there appeared to be unusual behavior in the upwash at the tip of the morphing wing. The AOA of the wing tip seemed to remain in a small range with

the local flow even when the tip was +14 degrees AOA to the tunnel flow (see Sec. 3).

Because of the inability of smoke to enter the boundary layer of the flow over the wind tunnel models and to due to the relatively high velocities needed it was decided to introduce a higher viscosity fluid to the boundary layer. A modified tempura paint with metallic flecks was applied to the models and tested with mixed results. The new fluorescent flow visualization fluid was easily entrained in the flow and could be photographed using ultraviolet light. This technique turned out to provide only some basic qualitative information (see [7] for full details). A general observation, which has not yet been fully explained, was that when the morphing wing was at high angles of attack with a control deflection between +3.5 and +7 degrees a scallop pattern developed along the outboard one third of the wing (see Fig. 8 and Sec. 3 for further details).

2.4 CFD Analysis

In order to gain greater insight into the flow physics of the morphing wing, CFD models of the various control positions at zero degrees angle of attack and seven degrees angle of attack were developed. In parallel, a validation model for the CFD simulations was also developed. There have been a number of computational studies on 3D wings. The one selected for CFD validation was the work by Kim and Rhee [9], which used a straight rectangular wing with a NACA 0012 airfoil profile at a Reynolds Number of 4.6 million. This study was selected because of its simple geometry and lower Re than other work. Kim and Rhee's study attempted to match the flow physics and data collected by Chow [10] of NASA Ames Research Center. Kim and Rhee created a model in Fluent which matched Chows experimental geometry. They evaluated a variety of meshing techniques as well as turbulence closure techniques. Models were developed which showed good agreement with Chows data.

A similar model was developed to be used as a validation model for current CFD simulations. Creation of the CFD validation

model was conducted in parallel with the creation of the computational morphing wing models in order to ensure the functionality of the meshing and modeling techniques used for the morphing models.

A grid structure was developed that worked well for both the morphing wing and the validation wing: a relatively fine triangular mesh on the wing which transitions to a Tet (mostly triangular) Hybrid Tgrid in the tunnel section. This technique was then applied to both the validation model and the morphing wing. Mesh quality was examined and it was found that certain ratios of fine wing face grid to the coarser volume grid used in the tunnel performed better than others. Certain ratios could not be generated without errors.

Boundary conditions were defined as a velocity inlet, a pressure outlet, generalized wall function for the wing surfaces and the tunnel walls. Justification could not be found for the use of the moving wall boundary condition for the tunnel walls that Kim and Rhee [9] used. However, this type of model was also investigated as well as both laminar and turbulent flow models.

Due to computing power limitations and the good performance shown by Kim and Rhee [9] the Spalart-Allmarus (S-A) turbulence model was used. This initial setup was followed by experimentation with a laminar model and with the use of a pressure based dynamic adaptive grid (Fluent). For validation, all models were run with the velocity inlet set at 170 ft/s and were limited to approximately 2.2 million cells due to available computing power.

In general, without using the moving wall boundary condition on the tunnel walls the prediction of C_L and C_D was high except for the laminar case which can only be poorly justified at a Reynolds number of 4.6 million and an AOA of 10 degrees. Due to these high predictions it was thought that the calculated wall effects were the cause for the high aerodynamic coefficients. In Chow's [10] experiments the relative large size of the wing model when compared to the wind tunnel test section may be the cause of the difficulty in fitting a turbulence model due to blockage and wall effects. As a test, two models were created

with the tunnel walls widened by 4 cord lengths. The results were excellent along with a model which used the pressure adaptive grid having the best results in duplicating pressure field seen in Chows data [10] and Kim and Rhee's models [9]. The results of this experiment were to validate both the grid cell intervals and the dynamic pressure adaptive grid which will be used on the morphing wing models.

The creation of CFD models for the morphing wing follows a similar path to that of the validation models. The initial models were constructed with a cell interval spacing of 5 mm in the wing and 25 mm in the wind tunnel which gives an overall cell count in the 1.6 million range. A velocity of 68 ft/s was set for the inlet boundary which matches one of the velocities used in the wind tunnel testing. The CFD model test section has the same dimensions as the wind tunnel, but the 46.5 inch test section length was tripled in order to aid in meshing and to give time for the flow to equilibrate before the outlet. Control positions at 0 degrees AOA and at 7 degrees AOA were built into 10 models (two angles of attack and 5 control positions) and were run using the S-A turbulence model.

The initial CFD models were over predicting both C_L and C_D for every condition when compared to wind tunnel data. Based on the low Re (375,000) and low angle of attack of the wing, use of the laminar model was investigated. In addition, the adaptive grid functionality was activated which added on average 160,000 grid cells to the wing model. (see [7] for full details). Use of the laminar model along with the adaptive grid brought both C_L and C_D in line with the wind tunnel data. C_L was still slightly high, but reasonable. C_L and C_D data for the various models is summarized in Table 2 and 3.

In general at zero degrees AOA the controls perform much as expected. The lift coefficient remained around zero. Both the laminar and turbulent models were in good agreement in behavior. The laminar models C_D values were lower in magnitude than the turbulent in all conditions. Drag values varied little at zero AOA for any data set. The laminar models varied between 0.014 - 0.017 and the turbulent model varied between 0.042 - 0.043.

Control behavior was much more interesting when lift was present at 7 degrees AOA. As far as lift, both data sets showed good agreement in magnitude and general behavior. The CFD models showed an increase in lift from the -7 degree control deflection through the +7 degree control deflection. The C_L values ranged from 0.51 - 0.59. Drag value magnitudes showed good agreement between the laminar and turbulent data in behavior while the S-A model produced higher C_D values. Both models showed an increase in C_D from the -7 degree control position to the +3.5 degree control deflection then decreased again when moving to +7 degree control position.

A region of significant interest is the tip region where control deflections occur. CFD pressure data showed that very little flow or pressure changes occurred in the root-ward two thirds of the wing during control deflections, but there were large changes near the tip. The tip region is also where most of the differences between the laminar and the S-A models occurred. At zero degree AOA both the laminar and turbulent models showed good agreement in the flow physics. The seven degree AOA laminar model predicts a region of reversed flow beginning near the root at the trailing edge which extends tip-ward, covering up to half the cord at the tip for extreme positive control deflections, where as the turbulent model predicts mostly attached flow through all the control positions. The models all showed an unusually high upwash at the tip when the wing was at a positive angle of attack. Even with -7 degree control deflection, the upwash adjusted to give the tip a positive AOA. With positive control deflections up to +7 degrees the upwash angle was greater than the control deflection.

As an example, Fig. 9 shows the static pressure on the wing top surface at 7 degree AOA and the two extreme control positions. At the -7 degree control deflection there was a region of low pressure air which extended from 2 inches from the root out 2/3 of the wing along about the 10% cord. There was a corresponding high pressure region on the lower wing surface directly below the leading edge which also ran out 2/3 of the wing and gently tapered toward the leading edge of the tip. At the -3.5 degree

control deflection the patterns were similar except both the high and low pressure regions of air extended another 10% toward the tip. At the 0 degrees control position both the high and low pressure pods extended to approximately 2 inches from the tip and both gently taper to the tip leading edge. At the +3.5 degree control deflection the low pressure pod extended to the tip and intensified by 60 Pa and began to rotate toward the leading edge. The high pressure air on the bottom of the wing extended to cover 1/3 of the tip. These trends continued as the control was moved to the +7 degree control deflection. The low pressure area intensified another 60 Pa and moved to cover the leading edge of the outboard 1/3 of the wing. The pressure region on the lower wing surface again had a gentle taper to the tip leading edge. In general, the most dramatic pressure changes occurred around the +3.5 degree control deflection.

To facilitate the study of wake flow and pressure structures 2D contour planes were generated perpendicular to the wind tunnel walls and the root. Close to the tip low pressures indicative of the core of a tip vortex were visible. This low pressure core structure intensified from the -7 degree control deflection until the +3.5 degree control deflection and then appeared to breakup rapidly as the control was moved to +7 degrees.

2.5 Flight Demonstrator

In order to show the feasibility of the WVU morphing mechanism a flight demonstrator was developed. The flight demonstrator design began with the wind tunnel morphing model as the initial design. The size of the demonstrator was determined based on the following factors: cost, time for construction and proper wing load with data acquisition system on board. To minimize cost and construction time the minimum size aircraft was desired while still being in a similar Reynolds number range as the wind tunnel tests.

The wing loading study and test glider experience lead to the determination that the wing loading should be below 1.3 lbs/ft², so the aircraft should have a wing area of at least 7 square feet considering structural and

propulsion weight. One of the previous WVU tailless flight demonstrators had a span of 7 feet, an area of 7.96 square feet and the PUL-10 type elevons. The experience with this aircraft and the ability to compare the flight characteristics lead to the decision to make the new morphing flight demonstrator with a 7 ft span. The additional wing area provided by the 7 ft span also made it possible to either add additional sensors and computer equipment or additional batteries for improved endurance.

Weight was a critical factor in this aircraft because it would be using an unproven control system so the lightest structure possible within cost constraints was developed. For brevity, many construction details have been omitted, but Guiler [7] has full details.

The original morphing mechanism design was modified to decrease weight and to increase the rigidity. The lessons learned from the earlier models indicated that the leading edge torque rod needs to be as large a diameter as possible to give it rigidity under aerodynamic loads. It was also determined that a much lighter, more rigid structure could be developed if the torque rod was replaced by a dedicated hinge rod in the leading edge and an actuator rod. The actuator rod has a bend designed into it which cams the morphing feathers to their desired control positions as it rotates in a +/- 30 degree arch.

Assembly of the morphing mechanism included a carbon hinge rod into the leading edge of the wing, an actuator rod that was inserted through the wing ribs and a 1" actuator arm that was installed to allow the servo to rotate the actuator rod. Then the morphing feathers and Teflon spacers were installed [7].

The original neoprene skin design was unsatisfactory for the flight demonstrator due to: 1) weight, 2) required actuator force and 3) ballooning of the skin [7]. These problems were solved by covering most of the morphing region with a flexible, but non-elastic polypropylene film with thin laytex strips placed between each feather. This combination of materials negated the higher load on the servo. The new skin also reduced the skin weight from 2.2 lb to 0.24 lbs. The final aircraft weight with data acquisition and propulsion was 10.0 lbs, which was 0.3lbs below the design estimate. Fig. 10 is a picture of

the WVU flight demonstrator ready for flight with the controls in trim position (see [7] for propulsion and battery information).

The morphing surfaces could be used together as an elevator or differentially for an aileron function or in any combination. In their 6 degree washed-out position the surfaces were capable of 12 degrees of twist up or down at a throw rate of 60 degrees in 0.24 seconds.

Take off was in less than 200 ft at approximately 30 mph. The aircraft climbed at 11 ft/sec. After several orbits around the airfield at 500 ft, the aircraft was flown level at a single throttle setting of 29 mph. At this velocity the Re is 375,000 which matched the wind tunnel data. Most testing was conducted between 22 and 40 mph. although toward the end of testing the aircraft reached 89 mph in a powered dive.

After a variety of climbs and dives, stall tests began at an altitude of 600 ft. The stall speed was determined to be approximately 12 mph with gentle nose down stall behavior. After the first set of stall tests the aircraft was allowed to glide producing a glide ratio of 3.8:1, with a 15 degree glide slope. This glide slope was used as an estimate of the lift over drag ratio which agreed well with wind tunnel testing. Then the aircraft was flown level in non-accelerating flight with a constant throttle setting at 36 mph. A thrust of 0.956 lbs was determined and the coefficient of lift and drag (C_L and C_D) for the demonstrator were estimated at an assumed 6 degree angle of incidence in level flight and aircraft weight of 10 lbs: $C_D = 0.043$, $C_L = 0.454$

To determine roll rate, the aircraft executed four consecutive rolls giving an average 378 degree/sec roll rate. Then the second set of stall tests was initiated to test tip stall. The pilot was unable to get tip stall initiated. The elevon equipped demonstrator could be put into a tip stall easily. The pilot noted that roll and yaw behavior was very similar to the elevon equipped aircraft, but pitch was approximately 1/3 less responsive.

3 Discussion of Results

An adaptive washout morphing mechanism with comparable control characteristics to a similar sized Horten-type swept wing tailless aircraft

has been developed. Wind tunnel and CFD testing indicates that increases in L/D up to 40% are possible with a morphing wing when compared to the elevon equipped model. The data collected was in a critical Reynolds number range as shown in Fig. 11. It is important to note that due to the taper ratio, Reynolds number varies from 67,340 to 505,048, from tip to the root. The mean aerodynamic cord was used for all Reynolds numbers presented. Fig. 10 shows the drag coefficient; lift coefficient and L/D as a function of Reynolds number for the elevon model; the test velocities are at a Reynolds number where C_D changes rapidly.

Data on the Horten-type wing displayed the unique aerodynamics designed into this type of wing to mitigate adverse yaw. At the control position with the highest C_L (#5), the C_D is unexpectedly the lowest and the yaw moment is negative. This behavior also has a Reynolds number dependence and was only evident at velocities greater than 15 m/s ($Re \sim 300,000$).

Flow visualization techniques using polyester tufts helped define some of the tip vortex behavior. The tufts indicated when the tip vortex died out and when it reversed with varying control positions. It could be seen that the local AOA at the wing tip was not as large as seen at the root of the wing and that the lift vectors at the tip may rotate forward in certain control position in order to reduce drag and reverse yaw locally.

Wind tunnel, flight demonstrator and CFD data corresponded fairly well in this study. Fig. 12 and 13 summarize coefficient of lift and drag data from the three sources.

At zero degree AOA the lift coefficient of the wing stays around zero for all three data sets. Both laminar and turbulent models are in good agreement, but both have slightly higher lift values than data from the wind tunnel. The laminar CFD C_D values match wind tunnel data very well in magnitude at this AOA. The S-A turbulent model greatly over predicted C_D . The wind tunnel and laminar models varied between 0.014 and 0.017.

Lift coefficients at 7 degrees AOA (Fig. 12), for both data sets, as well as the flight demonstrator data showed good agreement in magnitude and general behavior except that the

wind tunnel model showed a decrease in lift at the neutral control position. The CFD models showed an increase in lift from the -7 degree control deflection through the +7 degree control deflection. The C_L values from the CFD models are higher than the wind tunnel values: 0.51 to 0.59 compared to 0.41 to 0.49. The C_L value from the flight demonstrator fell in between the CFD and wind tunnel data points.

Drag value magnitudes showed good agreement between the laminar CFD model, the flight demonstrator and the wind tunnel data, while the S-A model over predicted C_D , as shown in Fig. 13. All models showed an increase in C_D from the -7 degree control position to the neutral position. CFD predicted C_D increasing to the +3.5 degree control deflection then decreasing while the wind tunnel data makes this downward turn following the neutral position.

The flow physics which cause the drag behavior present in the 7 degree AOA wing between the neutral and +7 degree control deflections was difficult to study. In general CFD shows the low pressure region on the wing top surface extending toward the wing tip, intensifying and rotating toward the leading edge with increasing control deflection. The high pressure air below the wing has a similar trend except that it reaches the wing tip before the +3.5 degree control position and then retreats again between +3.5 and +7 degree control positions, which may indicate that it is bleeding off the trailing edge before the tip. At the +3.5 degree control position the high pressure air covers most of the tip and has a very steep gradient. This may indicate that it is feeding the tip vortex. Pressure profiles at the tip indicate that the strongest tip vortex is at the +3.5 degree control position and then rapidly breaks up between +3.5 and +7. This breakup corresponds to a slight decrease in drag without any degradation on lift between these two control positions. This tip vortex change can clearly be seen in Fig. 14 (2D planes perpendicular to tunnel wall at wing tip).

Smoke flow visualization in the wind tunnel showed an unusually behaving upwash at the wing tip which tended to adjust itself to remain in a constant angle range to the wing tip

with a control deflection. CFD data showed the same phenomena. For example, the tip had a control deflection of +7 degrees and the wing has a +7 degree AOA which gave the tip +14 degree AOA to the tunnel flow yet the upwash altered the localized flow to be +7 degrees or less. The upwash was seen up to 4 tip cord lengths forward of the wing in certain conditions. The self-adjusting pressure field which is responsible for the upwash may be a factor in the pilot's inability to get the flight demonstrator to go into a tip stall.

There are two factors which may contribute to the slight increase in lift and decrease in drag when approaching the +7 degree control deflection. One is the breakup of the tip vortex and the other is the rotation of the extreme low pressure from the wing top to the outboard 1/3 of the leading edges, which may develop a pressure distribution that produces induced thrust at the wing tip. The unique flow and pressure distributions are caused by the combination of a large high lift root, the 35 degree sweep and the 4 degrees of dihedral. It is likely that this unique set of conditions would be hard to maintain at different velocity or Reynolds number ranges.

When the flow and pressure on the wing surface from the laminar CFD model is examined in the tip region, at a 7 degree angle of attack and at the +7 degree control position, unusual low pressure structures can be seen. Static pressure plots of the wing surface show valleys of low pressure which progress from the leading edge and curve toward the tip trailing edge. These low pressure valleys intersect the low pressure region which follows the leading edge to create a scallop pattern along the leading edge. (Fig. 15) This scallop pattern was also seen in the tempura paint flow visualization (Fig. 8), but was disregarded at that time because of a lack of understanding. When velocity vectors are overlaid on the pressure contours, it becomes obvious that rotational flow exists at the center of each of these scallops and the low pressure valleys. Though more work needs to be done on this phenomenon, these features appear to be vortex filaments generated on the leading edge. (Fig. 16)

4 Conclusions

This research project developed an adaptive washout morphing mechanism for the control of a swept wing tailless aircraft. The adaptive washout morphing mechanism was able to provide effective roll, yaw and pitch control for a swept wing tailless aircraft. This new control technique was experimentally and numerically compared to an existing elevon equipped tailless aircraft and has shown the potential for significant improvements over that system in terms of efficiency and improved lift/drag. The feasibility of this mechanism was also validated by designing, fabricating and testing a flight weight version which performed in much the same way of a conventional elevon system.

In the process of comparing the Horten type elevon equipped models and the morphing models, formal wind tunnel verification of wingtip induced thrust found in Horten (bell shaped lift distribution) type swept wing tailless aircraft was documented. The extreme downward elevon deflection results in the forward rotation of the lift vector at the tip, which counters adverse yaw. Wind tunnel data also indicated that this effect may only exist in a small velocity range for a given wing twist geometry. This would agree with the Horten test pilot's observation of problematic adverse yaw during many maneuvers.

Through the use of wind tunnel testing, flow visualization and CFD a more developed physical understanding of the highly complex flow developed in the control region of the morphing tailless aircraft has been developed. The data collected showed physical reasons for the phenomena observed in the morphing model, in particular for the control position that has the highest C_L with the lowest C_D .

This research also has given a rare comparison of low Reynolds number CFD data, wind tunnel data, wind tunnel flow visualization and free flight data. The exact same geometry and Reynolds number was used in all and the results agreed well with each other in the narrow range of test conditions. The viability and potential for efficiency gains have been documented and further research should be conducted in order to further characterize this

type of control and to explore the possibilities of using both variable sweep and adaptive washout which would move closer to natural flyers.

Acknowledgements

This work was supported through a NASA GSRP grant from NASA Dryden Research Center. The authors would like to thank Dr. Al Bowers for his help and guidance. The authors would also like to thank Dr. Karl Nickel for the helpful discussions on this work.

References

- [1] Northrop, John, K. "The development of all-wing aircraft," 35th Wilbur Wright Memorial Lecture, London, May 29, 1947.
- [2] Bowers, A. "Flying wing aerodynamics", April 1999.
- [3] George-Falvy, D. "A review of aerodynamic evaluation tests of the Horten IVa flying wing", Presented at the National Soaring Museum Wing Symposium, Elmira, NY, July 17, 1997.
- [4] Horten, R. and Selinger, P. "Nürflügel-Die Geschichte der Horten-Flugzeuge 1933-1960", H. Weishaupt Verlag, Graz, Austria, 1993.
- [5] Nickel, K. and Wohlfahrt, M. *Tailless aircraft in theory and practice*. American Institute of Aeronautics and Astronautics, Inc., Washington, D.C., 1994.
- [6] Hepperle, M. "Airfoil design for light tailless airplanes", http://www.mh-aerotoools.de/airfoils/nf_8.htm, 2004.
- [7] Guiler, R.W. *Control of a swept wing tailless aircraft through wing morphing*. PhD dissertation, West Virginia University, 2007.
- [8] Gerontakos, P. and Lee, T. Near-field tip vortex behind a swept wing model. *Experiments in Fluids*, Vol. 40, No. 1, pp. 141-155, 2006.
- [9] Kim, S.E., and Rhee, S.H. "Prediction of tip-vortex flow past a finite wing," AIAA-2005-58, 43rd AIAA Aerospace Sciences Meeting and Exhibit, Jan. 2005.
- [10] Chow, J., Zilliac, G., and Bradshaw, P. "Turbulence measurements in the nearfield of a wingtip vortex," NASA Technical Memorandum 110418, February, 1997.

Copyright Statement

The authors confirm that they, and/or their company or institution, hold copyright on all of the original material included in their paper. They also confirm they have obtained permission, from the copyright holder of any third party material included in their paper, to publish it as

part of their paper. The authors grant full permission for the publication and distribution of their paper as part of the ICAS2008 proceedings or as individual off-prints from the proceedings.

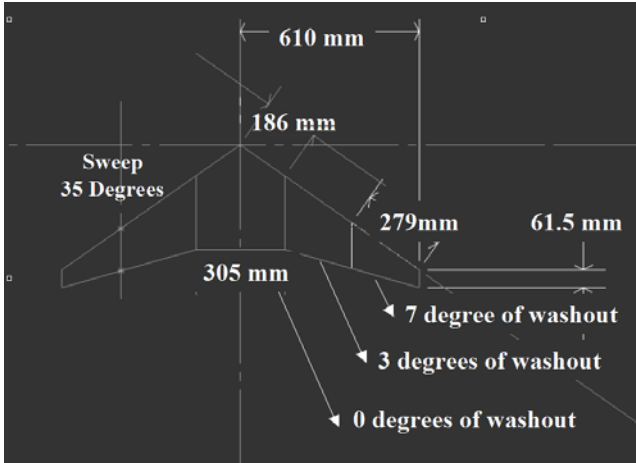


Fig. 1. Final basic aerodynamic non-morphing configuration.

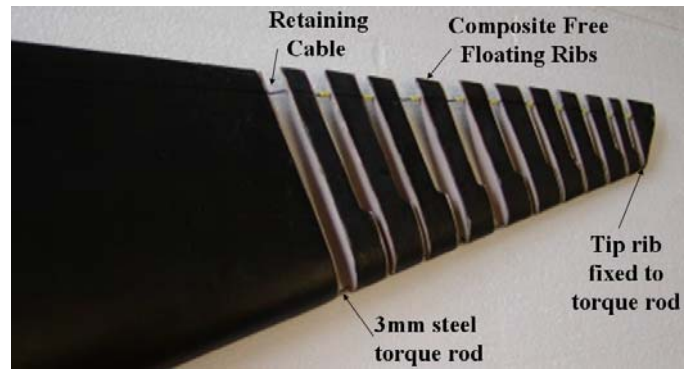


Fig. 2. Basic modified adaptive wash-out mechanism structure.

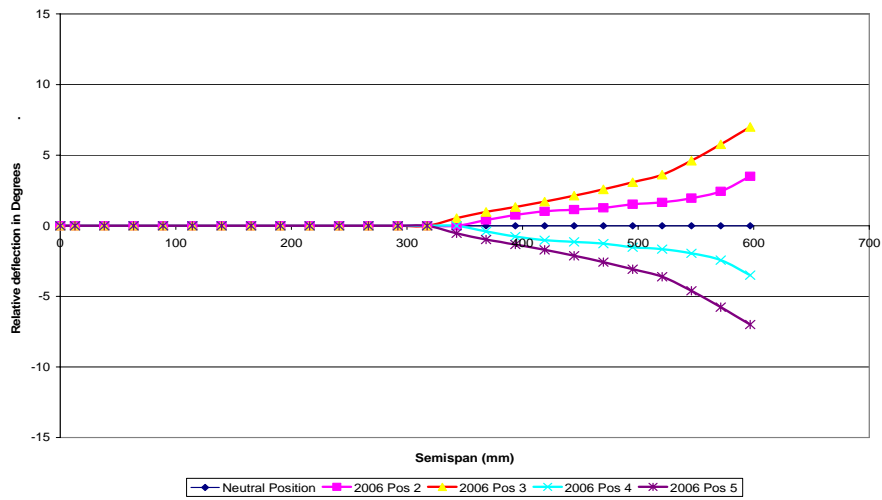


Fig. 3. Trailing edge curvature within Nylon monofilament. Note leading edge remains fixed.

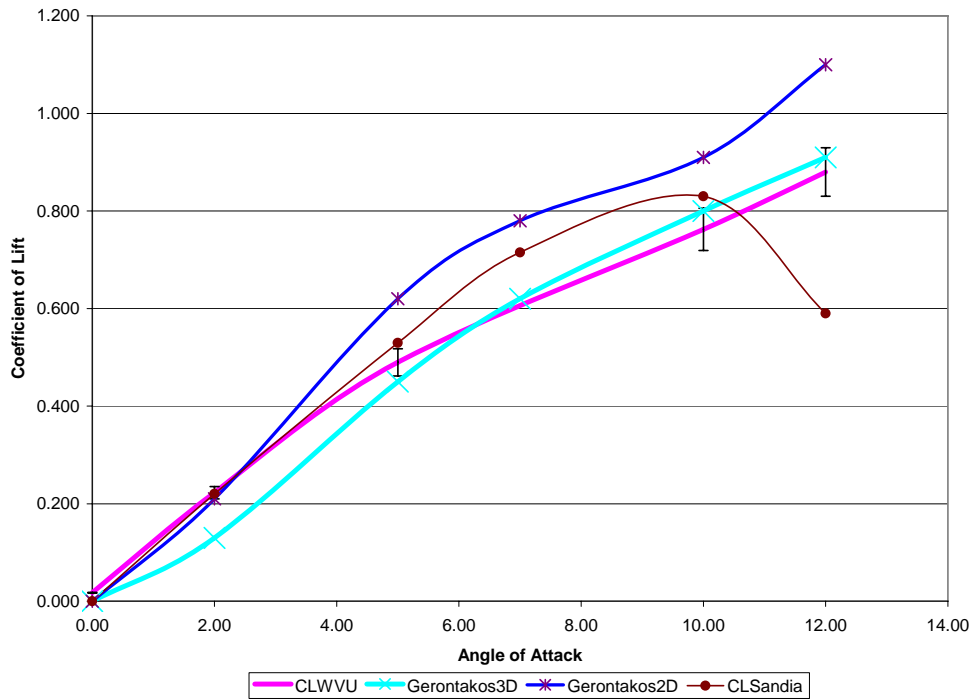


Fig. 4. Coefficient of lift data comparison between WVU NACA 0015 validation model data, Gerontakos data and 2D Re 160000 data from Sandia National Labs.

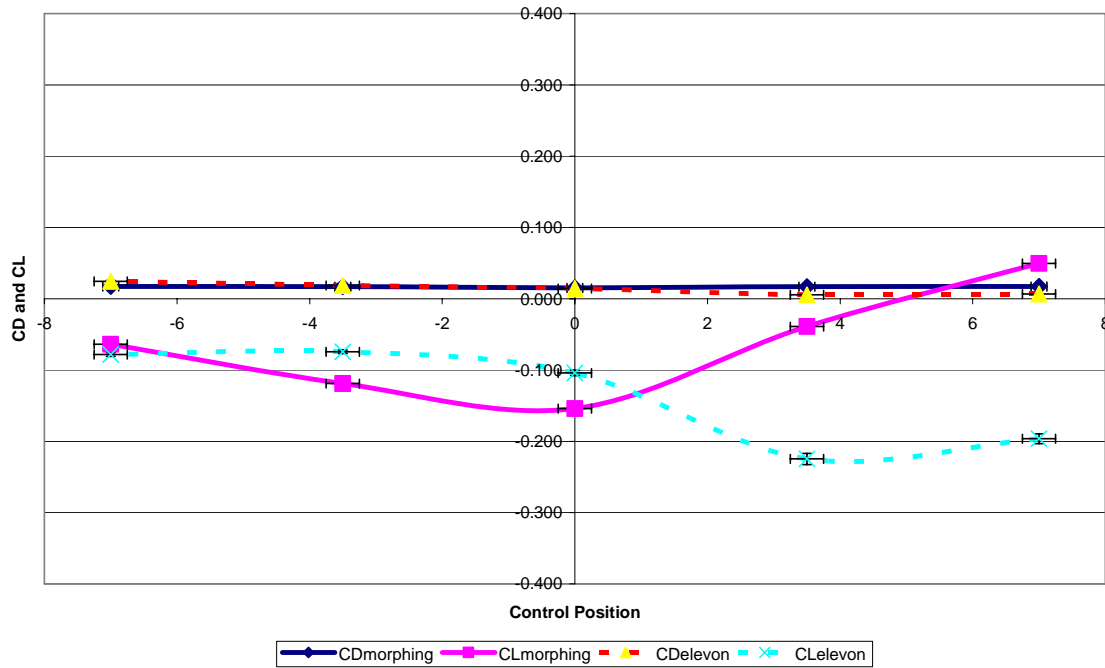


Fig. 5. Experimental C_L and C_D aerodynamic coefficients for both wings at 0 degrees AOA and 68ft/sec (21 m/s).

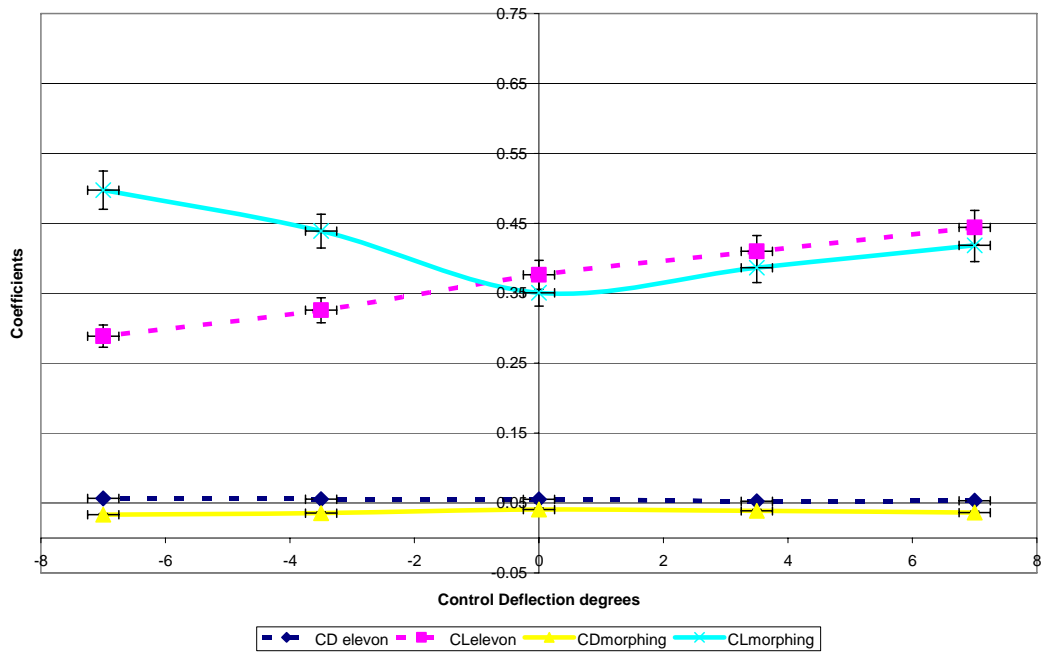


Fig. 6. Experimental C_L and C_D for both wings at 7 degrees AOA and 68 ft/sec (21 m/s).

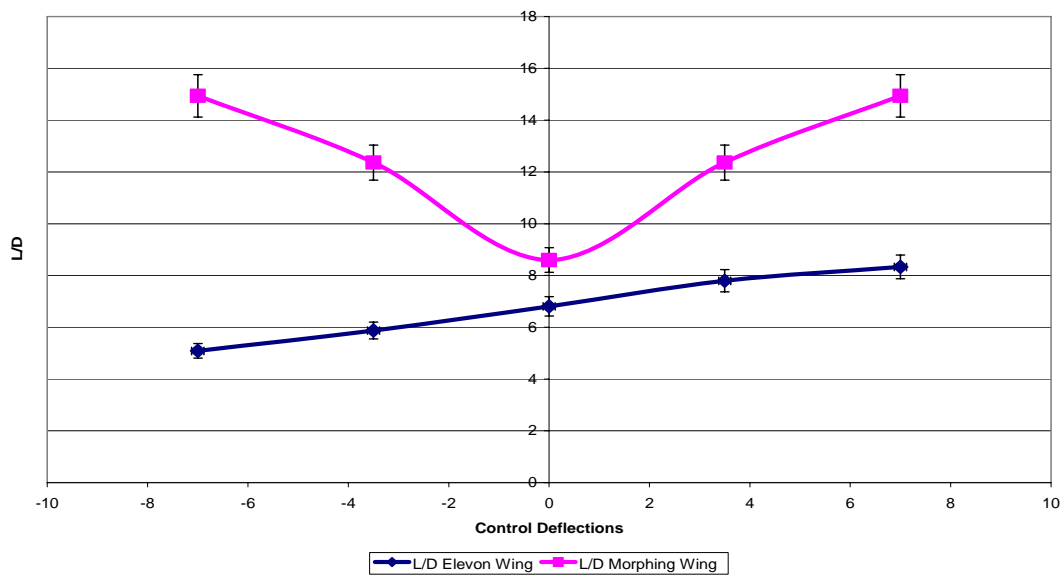


Fig. 7. Experimental L/D ratios for both wings at 7 degrees AOA and 68ft/sec (21 m/s).

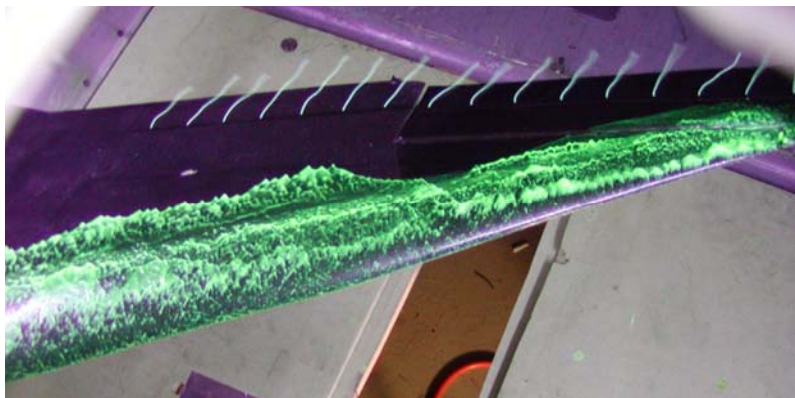


Fig. 8. Wing with florescent flow visualization fluid at 7 degrees AOA, control position 5 and 21 m/s.

Table 2. C_L and C_D of various Fluent models simulating Chow’s experiments [10].

| Model | Mesh and Boundaries | C_L | C_D | Wing Pressure Contours |
|---|--|-------|-------|------------------------------|
| Chow (Experimental Data) | NA | 0.51 | 0.077 | Baseline - 220 Pressure Taps |
| NACA0012REVA626 | 1.6 million cells Spalart-Allmaras, 2nd Order | 0.78 | 0.1 | |
| NACA0012REVA629 used adaptive boundary grid on wing and dynamic pressure gradient adaptive grid | 1.6 million cells Spalart-Allmaras, 2nd Order | 0.76 | 0.131 | |
| NACA 0012Extended701 Moved walls out by 4 cord lengths | 1.9 million cells Spalart-Allmaras, 2nd Order | 0.425 | 0.079 | Excellent match |
| NACA0012709 used adaptive boundary grid on wing and dynamic pressure gradient adaptive grid | 0.8 million cells Spalart-Allmaras, 2nd Order | 0.76 | 0.106 | |
| NACA0012REVA629709 used adaptive boundary grid on wing and dynamic pressure gradient adaptive grid | 2.17 million cells Spalart-Allmaras, 2nd Order | 0.76 | 0.131 | |
| NACA0012Extended710 used adaptive boundary grid on wing and dynamic pressure gradient adaptive grid | 2.17 million cells Spalart-Allmaras, 2nd Order | 0.43 | 0.081 | Excellent match |
| NACA0012709AL used adaptive boundary grid on wing and dynamic pressure gradient adaptive grid | 2.17 million cells Laminar, 2nd Order | 0.67 | 0.062 | Excellent match |

Table 3. Lift and drag from wind tunnel experiments (C_D/C_L -WT), turbulent (C_D/C_L -S-A) and laminar CFD (C_D/C_L -LAM)models at 0 and 7 degrees AOA.

| AOA 0 degrees | Wind Tunnel Data | CFD S-A | | CFD LAM | | |
|------------------|------------------|----------|-----------|-----------|-----------|-----------|
| | C_D WT | C_L WT | C_D S-A | C_L S-A | C_D LAM | C_L LAM |
| Control Position | | | | | | |
| -7 | 0.017 | -0.064 | 0.043 | -0.019 | 0.014 | -0.022 |
| -3.5 | 0.017 | -0.119 | 0.042 | -0.006 | 0.014 | -0.008 |
| 0 | 0.015 | -0.154 | 0.043 | 0.007 | 0.015 | 0.004 |
| 3.5 | 0.017 | -0.039 | 0.042 | 0.023 | 0.014 | 0.021 |
| 7 | 0.017 | 0.050 | 0.043 | 0.037 | 0.015 | 0.035 |
| AOA 7 degrees | Wind Tunnel Data | CFD S-A | | CFD LAM | | |
| | C_D WT | C_L WT | C_D S-A | C_L S-A | C_D LAM | C_L LAM |
| Control Position | | | | | | |
| -7 | 0.036 | 0.418 | 0.068 | 0.504 | 0.031 | 0.540 |
| -3.5 | 0.039 | 0.386 | 0.069 | 0.517 | 0.033 | 0.550 |
| 0 | 0.041 | 0.351 | 0.070 | 0.530 | 0.036 | 0.560 |
| 3.5 | 0.036 | 0.439 | 0.078 | 0.560 | 0.041 | 0.590 |
| 7 | 0.033 | 0.497 | 0.070 | 0.560 | 0.040 | 0.590 |

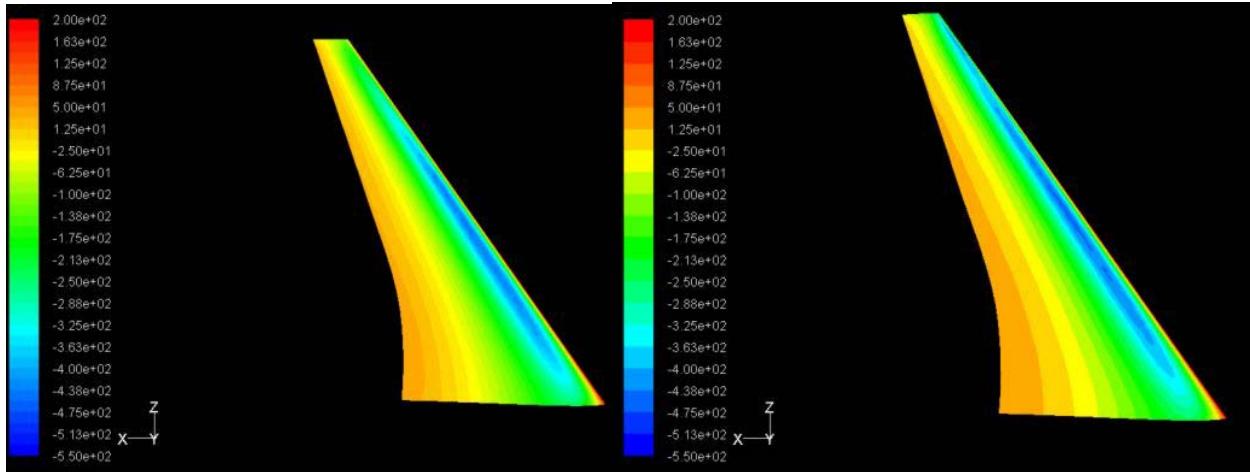


Fig. 9. Static pressures on the wing top at 7 degrees angle of attack and a -7 degree control deflection (left) and a +7 degree control deflection (right).



Fig. 10. WVU 7' morphing flight demonstrator ready for flight.

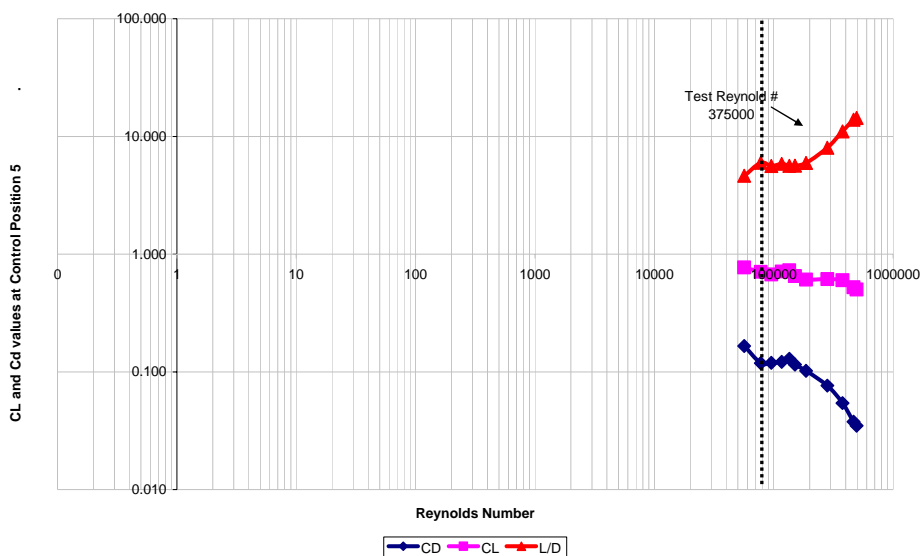


Fig. 11. CD, CL and L/D at increasing Re for the elevon equipped wing at 7 degree AOA and in control position 5.

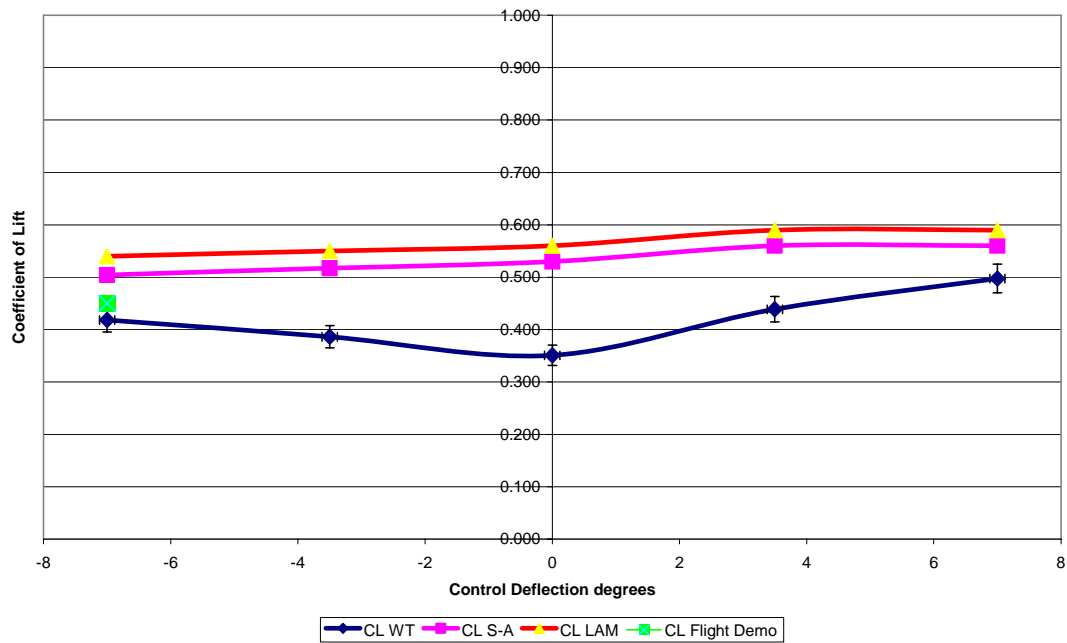


Fig. 12. Coefficient of lift comparison between wind tunnel data, a CFD model using S-A turbulence model and a laminar flow CFD model at 7 degrees angle of attack.

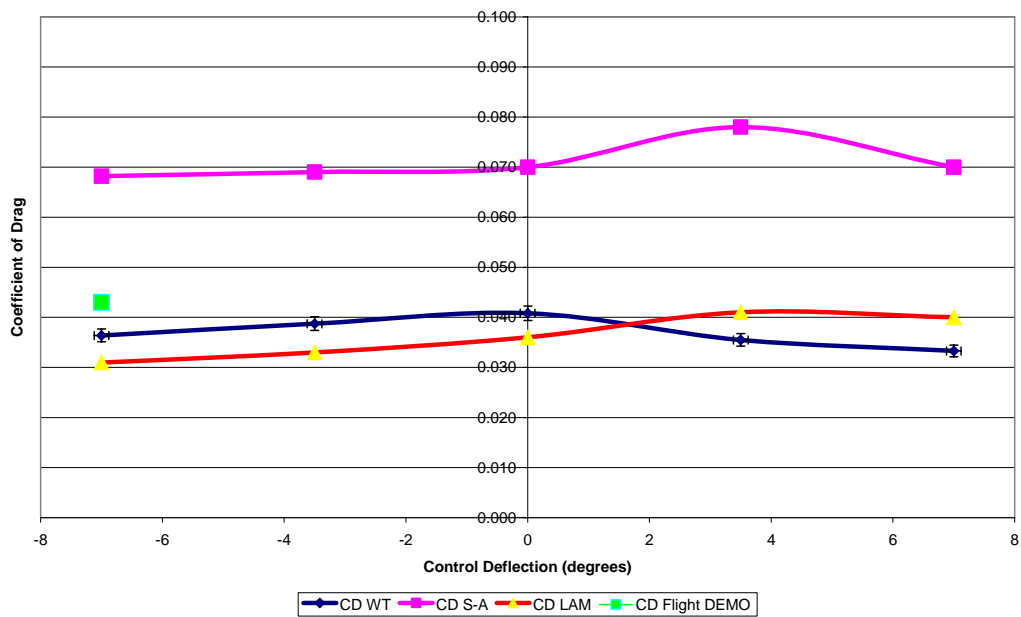


Fig. 13. Coefficient of drag comparison between wind tunnel data, a CFD model using S-A turbulence model and a laminar flow CFD model at 7 degrees angle of attack.

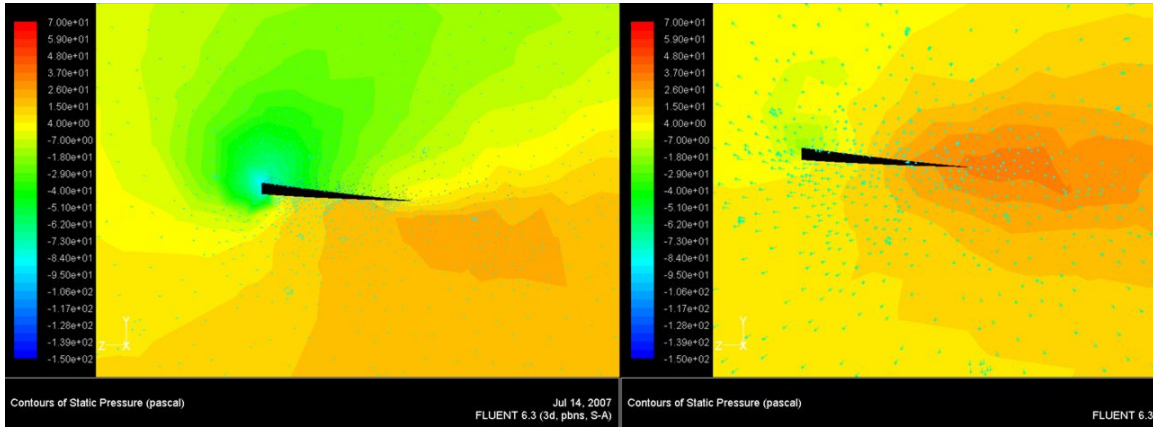


Fig. 14. Low pressure wing tip core structures at +3.5 degree control deflection (left) and +7 control deflection (right).

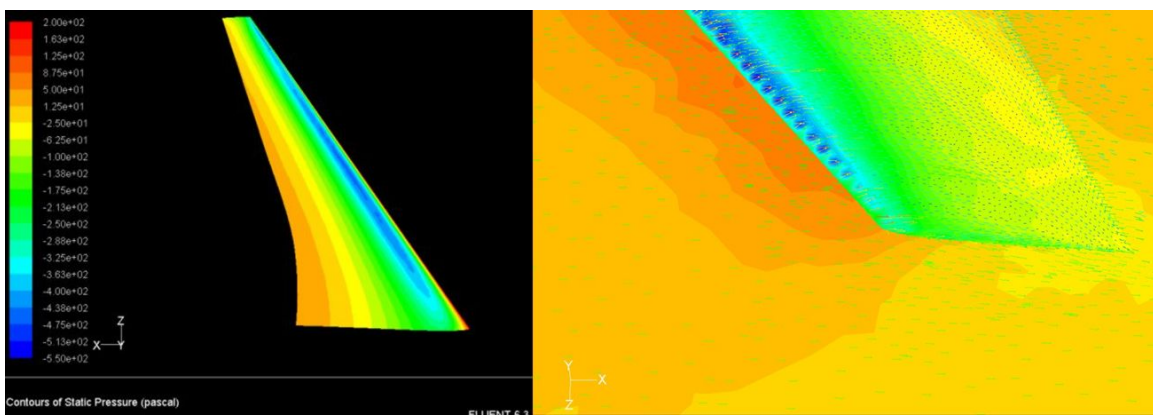


Fig. 15. Static pressure field on top wing surface and near the tip at a +7 degree control deflection with the wing at 7 degrees angle of attack.

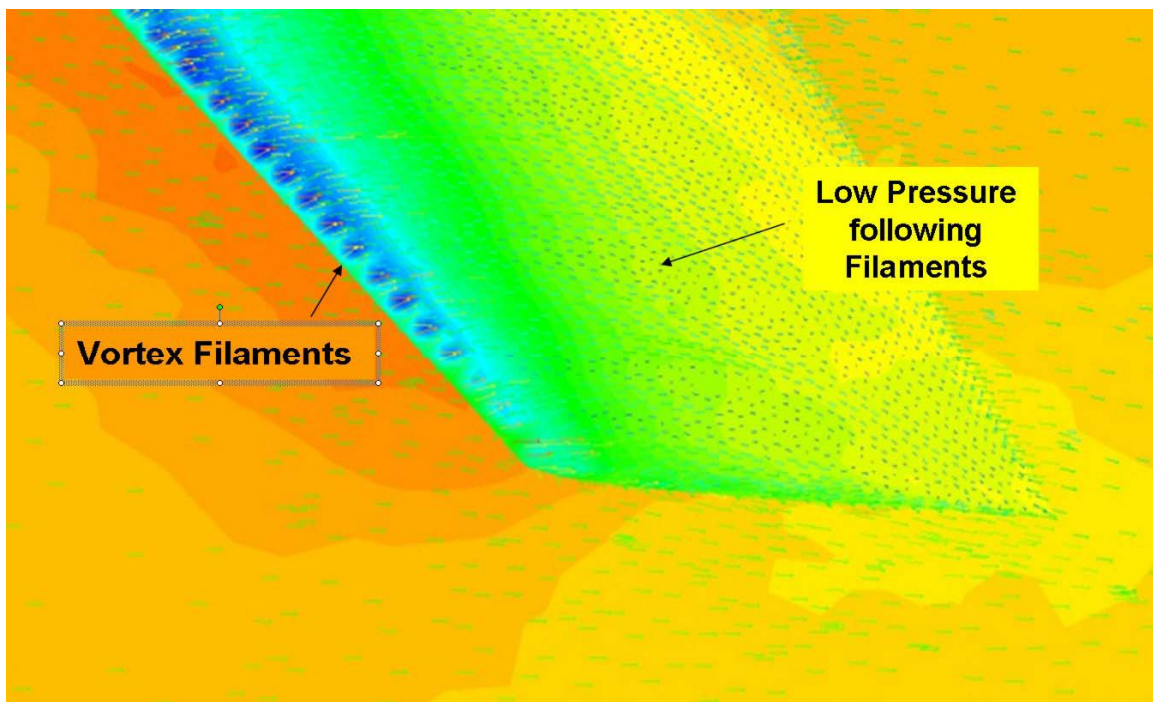


Fig. 16. Static pressure and velocity flow vectors just above the wing tip surface.